arXiv:1509.08249v1 [cond-mat.supr-con] 28 Sep 2015

Superconductivity and Magnetism in Noncentrosymmetric RhGe

A. V. Tsvyashchenko,* V. A. Sidorov, A. E. Petrova, L. N. Fomicheva, and I. P. Zibrov
L. F. Vereshchagin Institute for High Pressure Physics, Russian Academy of Sciences, 142190, Moscow, Troitsk, Russia

V. E. Dmitrienko
A. V. Shubnikov Institute of Crystallography, Russian Academy of Sciences, 119333, Moscow, Russia

RhGe synthesized at high pressure is crystallized in noncentrosymmetric cubic structure of the $B20$ type. Measurements of the electrical resistivity and magnetization demonstrate a superconducting state below $T_c \sim 4.5$ K and a weak ferromagnetism below $T_m \sim 140$ K. Specific heat data confirm the bulk nature of superconductivity in this ferromagnetic superconductor. The superconducting region forms a dome on the P-T diagram with a maximum of T_c near 4 GPa. *Ab initio* simulations suggest that the observed weak magnetization emerges from the pronounced spin polarization with magnetic quadrupole and toroidal moments located at Rh and Ge sites.

With the discovery of the superfluid phases of ^{3}He [1, 2] understanding of superconductivity in terms of a condensate of Cooper pairs, with the Cooper pairs forming due to electron-phonon interactions [3] began to change. It was found that the heavy-fermion compounds containing f-elements are prime candidates for unconventional superconductivity with complex order parameter symmetries [4]. These compounds can be put in close analogy with the heavy Fermi liquid ^{3}He, and analogous interactions in that case with high probability lead to spin-triplet, magnetically mediated, superconductivity [5].

The central issue for heavy-fermion superconductors is the question of the coexistence of superconductivity and magnetism. First time the superconductivity (in a limited pressure range) was discovered on the border of itinerant-electron ferromagnetism below 1 K, in a pure system, UGe_2 [6]. Superconductivity of the ferromagnet URhGe [7] and UCoGe [8] observed at normal pressure was also considered in terms of the magnetic and spin triplet pairing as for UGe_2.

However for the superconducting condensate an interesting question is not only the mechanism of pairing and the symmetry [9, 10]. According to Refs. [11, 12] in the absence of inversion symmetry the order parameter becomes a mixture of spin-singlet and spin-triplet components, which leads, for instance, to the Knight shift attaining a nonzero value at $T = 0$. The striking examples of such noncentrosymmetric superconductors are $CePt_3Si$ [13, 14] and UIr [15].

On the other hand there were unsuccessful attempts to observe superconductivity under high pressure on the border of itinerant-electron ferromagnetism in a noncentrosymmetric compound without f-elements (for example MnSi) [16, 17].

The aim of this Letter is to report on unconventional superconductivity and long range high temperature magnetic order in the high pressure cubic phase of RhGe (the $B20$ type [18]), to evaluate parameters characterizing the superconducting state and to discuss possible scenarios of magnetic ordering.

The MX compounds of the transition metals (M) (e.g., Mn, Fe, Co) with metalloids (X) (e.g., Si, Ge) which crystallize in the FeSi ($B20$) structure type continue to attract attention in the field of solid state physics due to the existence of rich magnetic and electronic phenomena. In the silicides there have been found long-period helical structures [19], quantum phase transitions and partial order in the high-pressure phase [20, 21], vortex-like spin textures or skyrmions [22, 23], which can be controlled by an electric current, inducing a topological Hall effect [24–26].

The cubic high pressure phase of MnGe [27] shows the highest magnetic moment among the $B20$ metals [28, 29] which around 6 GPa transforms from a high-spin to a low-spin state [30]. Germanides with the $B20$ structure have stronger ferromagnetic properties than the silicides [31, 32], as required to exploit their chiral magnetism.

Polycrystalline samples of RhGe cubic phase were synthesized at 8 GPa in the toroidal high-pressure apparatus [33] by melting reaction between Rh and Ge. The purity was 99.99% for Rh and 99.999 % for Ge. The pellets of well-mixed powdered constituents were placed in rocksalt pipe ampoules and then directly electrically heated to 1700 K. Then the samples were quenched to room temperature before the applied pressure was released. Crystal structure was determined from x-ray data (Cu Kα_1 radiation, Guinier camera - G670, Huber) and found to be simple cubic, the space group $P2_13$ (No. 198) with a =4.85954(2) Å ($V = 114.758(1)$ Å^3), isotypic with the crystal structure of FeSi ($B20$) without the inversion symmetry. The $B20$ structure has 8 atoms per unit cell. Both Rh and Ge are located at the Wyckoff positions ($4a$) with coordinates (u, u, u), ($u + 0.5$, $0.5 - u$, $-u$), ($-u$, $0.5 + u$, $0.5 - u$), and ($0.5 - u$, $-u$, $0.5 + u$) where u(Rh) = 0.12809(11) and u(Ge) = 0.83368(13). Rietveld refinements (GSAS [34, 35]) revealed phase purity of the polycrystalline material used for bulk property measurements. The sites occupancy of Rh and Ge was also de-

*Electronic address: tsvyash@hppi.troitsk.ru

termined from the Rietveld analysis (Rh/Ge $\sim$ 1/0.986 for this sample). More details can be found in Supplementary Materials [36].

Basic physical properties of this polycrystal are displayed in Figs. 1, 2, 3. The electrical resistivity and specific heat were measured with the Quantum Design PPMS instrument. Magnetic properties were measured with VSM inserted in PPMS. Temperature dependence of the electrical resistivity $\rho(T)$ of $RhGe_{0.986}$ (Fig. 1) is of metallic type with gradual saturation below 10 K. In the range 4.5-30 K $\rho(T)$ follows the dependence $\rho(T) = \rho_0 + AT^3$. This type of dependence was found in a number of transition metal compounds and is explained by phonon assisted interband s-d scattering [37]. Below 10 K, a T^2 dependence of $\rho(T)$ typical for the Fermi liquid was found in FeGe and MnGe [38]. At 4.5 K resistivity starts to drop and finally goes to zero at 2.6 K. Thus RhGe is the first superconductor in the series of MX compounds with the $B20$ structure lacking inversion symmetry. Earlier superconductivity with $T_c = 0.96$ K was reported for an ambient pressure phase of RhGe having the orthorhombic ($B31$) MnP-type structure [39]. Nevertheless for RhSi ($B20$) the superconductivity above $T_n = 0.35$ K was not detected [39]. The inset (a) in Fig. 1 shows $\rho(T)$ around the superconducting transition in different magnetic fields up to 3.5 kOe for $RhGe_{0.986}$. We estimated dH_{c2}/dT at T_c as -0.65 kOe/K. The shape of $\rho(T)$ near the superconducting transition may indicate the presence of two superconducting phases.

The bulk nature of the transition is confirmed by the specific heat measurements (inset (b) in Fig. 1). The bold straight line in the plot C/T vs T^2 is the best fit of data between 4 and 7 K and represents the contribution from phonons and electrons in the normal state. The electronic specific heat coefficient $\gamma = 2.9$ mJ/(mol·K^2) allows one to classify RhGe as a normal metal with weak electronic correlations. For magnetic MnGe, FeGe the coefficients γ are 16 and 9 mJ/(mol·K^2), respectively and for nonmagnetic CoGe $\gamma \sim 0$ mJ/(mol·K^2) [38]. The jump of the specific heat takes place at 2.6 K where resistivity goes to zero. Also small deviation between the bold line and experimental data may indicate on the contribution of superconducting phase to the specific heat below 4 K. The jump of the specific heat at the superconducting transition is small $\Delta C/\gamma T_c \sim 0.16$, and well below the BCS value $\Delta C/\gamma T_c = 1.43$. A reduced value of the specific heat jump at T_c may arise if only some parts of the Fermi surface have non-zero superconducting gaps, while the others remain gapless. Similar small jump $\Delta C/\gamma T_c = 0.25$ was found in the noncentrosymmetric antiferromagnetic superconductor $CePt_3Si$ [13] and in the ferromagnetic superconductor UGe_2 with the maximum of $\Delta C/\gamma T_c \sim 0.29$ and the maximum of $T_c = 0.6$ K reached at a critical pressure 1.22 GPa [40].

Notice that according to the measurements of magnetic susceptibility $\chi(T)$ in applied field $H = 300$ Oe (Fig. 2) RhGe becomes weakly ferromagnetic below $T_m \sim 140$ K and superconducting below 4.1 K. Measurements at

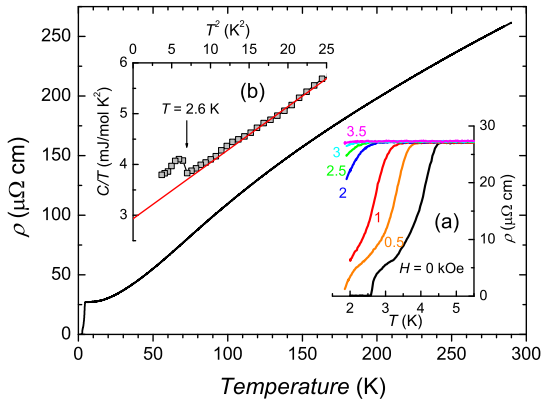

FIG. 1: Temperature dependence of the electrical resistivity of $RhGe_{0.986}$. Inset (a) - temperature dependences of resistivity in different magnetic field around the superconducting transition. Inset (b) - temperature dependence of the specific heat (in the form C/T vs T^2) of RhGe around the superconducting transition.

2.5 K (Fig. 3) show the picture of magnetization typical for a ferromagnetic superconductor, demonstrating the coexistence of superconductivity and ferromagnetism at 2.5 K. Magnetic moment of $RhGe_{0.986}$ is saturated at the level of 0.023 emu/g ($\sim$0.0007 μ_B/f.u.) in magnetic fields above 70 kOe. This extremely small value of saturation moment should be compared with an effective magnetic moment in the paramagnetic state $\mu_{eff} = 1.18$ μ_B/f.u. found from the slope of a dependence $\chi^{-1}(T)$ (inset in Fig. 2). Thus, RhGe is a weak itinerant ferromagnet, but with a rather strong magnetic exchange ($T_m \sim 140$ K).

We have measured the low field ($\sim$1 Oe) magnetic ac-susceptibility to estimate the superconducting volume fraction of RhGe compared to typical BCS-type superconductor (Pb). Sample of RhGe and a piece of Pb with external dimensions close to those of RhGe sample were cooled down to 1.7 K in a home-made coil system. We tested $RhGe_{0.986}$ and $RhGe_{0.989}$ samples. For both samples the magnitude of diamagnetic signal below T_c was similar to that produced by Pb at 7.2 K. It was also found that the appearance of superconductivity is sensitive to sample composition and is favorable for samples close to stoichiometric RhGe. The $RhGe_{0.98}$ sample though has not displayed superconducting properties.

Pressure effect on superconductivity was studied for another superconducting sample of $RhGe_{0.989}$. Temperature dependences of the electrical resistivity $\rho(T)$ of $RhGe_{0.989}$ around the superconducting transition at different hydrostatic pressures are shown in Fig. 4. Clamped toroid-type pressure cell with a liquid pressure medium [41] was used for this experiment. The width of the superconducting transition does not depend on hydrostatic pressure. The superconducting temperature T_c

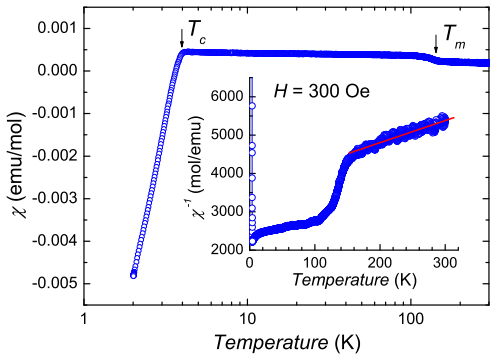

FIG. 2: Temperature dependence of the magnetic susceptibility of $RhGe_{0.986}$. The inset shows temperature dependence of the inverse susceptibility. The bold red line in the inset is a linear fit of data above the magnetic transition.

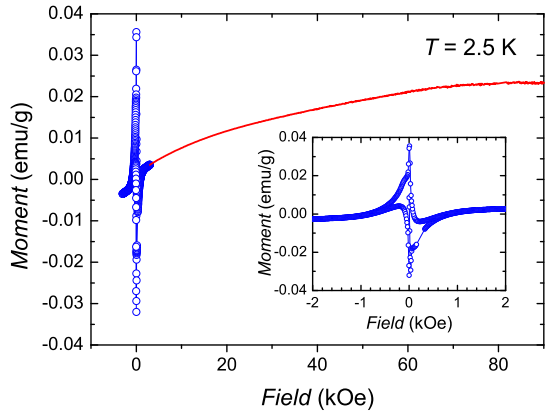

FIG. 3: Field dependence of the magnetization of $RhGe_{0.986}$ at 2.5 K. The inset shows the enlarged plot of magnetization at low fields.

increases first at high pressure at a rate $dT_c/dP = 0.15$ K/GPa but above 4 GPa T_c begins to decrease.

Structural, electronic and magnetic properties of the RhGe crystals of the $B20$ and MnP types were quantitatively evaluated with the Quantum ESPRESSO package developed [42] for the density-functional-theory (DFT) computations. The exchange-correlation functional with the generalized gradient approximation (GGA) of the Perdew-Burke-Ernzerhof type was chosen.

The scalar relativistic pseudopotentials were used for structure optimization (all the pseudopotentials were downloaded from the Quantum ESPRESSO data base [43]). To speed up the calculations, we used the symmetrized k-points: $6\times6\times6$ mesh for cubic $B20$ structure and $6\times10\times6$ for orthorhombic MnP-type structure. The plane-wave basis for wavefunctions had the cut-off energy of 40 Ry and the density cut-off energy was 440 Ry. The

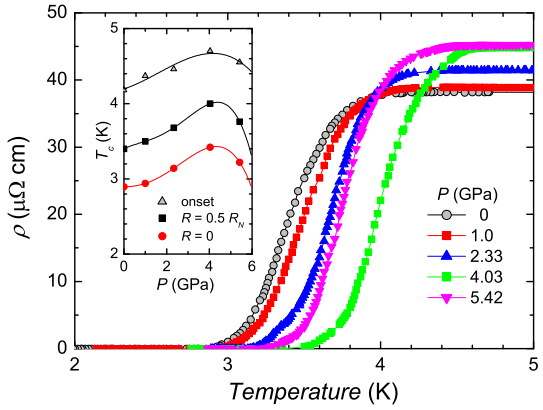

FIG. 4: Temperature dependence of the electrical resistivity of $RhGe_{0.989}$ near the superconducting transition at different pressures. The inset shows the P-T diagram of superconductivity in RhGe.

calculated energy-vs-volume dependence for RhGe is discussed in the Supplementary Materials. The $B20$ structure is more dense and it becomes energetically favorable for pressure above circa 8 GPa (at $T = 0$).

Fully relativistic GGA pseudopotentials were used for searching possible non-collinear magnetic structures with the spin-orbit interaction. The magnetic effects have been found to be very subtle in the case of the so-called ultra-soft potentials and we will not present correspondent simulations. It has been found that the final results do not change much for the $k \times k \times k$ between $8 \times 8 \times 8$ and $10 \times 10 \times 10$ and for the wavefunction cut-off energy between 40 Ry and 80 Ry. The pictures of the magnetization distribution $\mathbf{M}(\mathbf{r})$ presented below have been obtained for the $9 \times 9 \times 9$ mesh and the 40 Ry cut-off energy.

A typical example of the relaxed magnetization distribution inside a unit cell is shown in Fig. 5. The most interesting features are the small neighboring regions with plus and minus magnetizations along x-, y-, and z-directions. The shapes of the regions are typical of the p electronic states and their sizes scale with Z^{-1} as expected ($Z_{Rh}/Z_{Ge} \approx 1.4$). The orientations of the regions are different for different atoms in accordance with the orthorhombic symmetry $P2_12_12_1$ (instead of cubic $P2_13$ because of the uniaxial initial magnetization). The calculated total magnetization is rather small and directed along z, $|\langle\mathbf{M}(\mathbf{r})\rangle| \approx 0.0077\ \mu_B$, whereas the average absolute magnetization $\langle|\mathbf{M}(\mathbf{r})|\rangle \approx 1.0\ \mu_B$. We see that $\langle|\mathbf{M}(\mathbf{r})|\rangle \gg |\langle\mathbf{M}(\mathbf{r})\rangle|$, which means mainly 'antiferromagnetic' distribution of the magnetization. The absolute magnetization can be better characterized by the tensor of magnetization directions $D_{ik} = \langle M_i(\mathbf{r})M_k(\mathbf{r})\rangle$. However for the whole unit cell this tensor is almost spherically symmetric and does not tell much about the details of $\mathbf{M}(\mathbf{r})$.

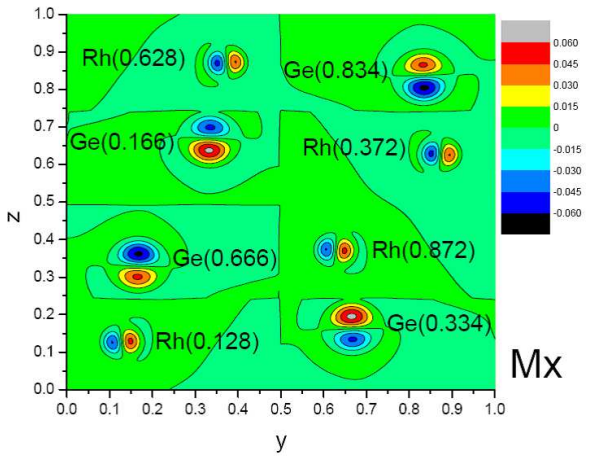

FIG. 5: Magnetic ordering in the RhGe unit cell: the space distribution of the M_x-magnetization around Rh and Ge atoms viewing along the x-axis (Quantum Espresso simulations). Similar patterns for the M_y- and M_z-components can be found in Supplementary Materials [36]. The figure is composed from 8 patches showing the magnetization in the yz-planes passing through the centers of corresponding atoms at 8 different x-levels; the atomic symbols and the x-levels are indicated in the figure. The boundaries between the patches are the straight lines: y=0.5, z=0.25, z=0.5, and z=0.75. The color scale palette is in arbitrary units.

For quantitative characterization of atomic magnetization we calculated different magnetic quantities for spheres around atoms. The radius of the spheres is chosen equal to 0.64 Å or 0.13 in the crystallographic units; see Fig. 5, which for the Rh atom roughly corresponds to the distance from the atom center to the unit cell boundary at the down-left corner. Obviously such spheres include the most interesting features of the magnetization distribution. The total volume of 8 spheres is only 7.8% of the unit cell. In the following we present results for Rh and Ge atoms at standard positions (at u, u, u). Data for the other sites can be obtained by corresponding symmetry transformations.

We have found that the atomic magnetization averaged over the sphere is $\langle \mathbf{M}(\mathbf{r})\rangle_{sph} = (170, 55, 20)\cdot 10^{-4}\mu_B$ for Rh and $(2, -4, -3)\cdot 10^{-4}\mu_B$ for Ge. It is interesting that for Rh the average atomic moment is directed mainly in x-direction whereas for Ge the x, y, and z components are comparable. However after summation over four RhGe units the x and y components almost vanish and only z magnetization survives providing almost 90% of the total ferromagnetic magnetization. In contrast, the absolute magnetization inside the spheres gives only 40% of the absolute magnetization, $\langle|\mathbf{M}(\mathbf{r})|\rangle_{sph} = 0.04\mu_B$ per Rh and 0.06 μ_B per Ge. The remaining 60% is an itinerant magnetization distributed in 92% of the unit cell volume.

The spatial distribution of magnetization inside the atomic spheres can be characterized by a non-symmetric tensor $Q_{jk} = \langle r_j M_k^{'}\rangle_{sph}$ where $\mathbf{M}^{'}(\mathbf{r}) = \mathbf{M}(\mathbf{r}) - \langle \mathbf{M}(\mathbf{r})\rangle_{sph}$. This tensor violates both T- and P-invariance [44] and can appear, for instance, if a p-state is admixed to an s-state. The symmetric part $(Q_{jk} + Q_{kj})/2$ is the magnetic quadrupole moment of the atom and the antisymmetric part $(Q_{jk} - Q_{kj})/2$ is equivalent to the vector of atomic toroidal moment $\mathbf{T} = \langle \mathbf{r} \times \mathbf{M}^{'}(\mathbf{r})\rangle_{sph}$. It is interesting that there is a non-zero scalar part Q_{jj} arising from the spin hedgehog pattern around each atom [45]: Q_{jj} is of about $1.5\cdot 10^{-4}$ μ_B for Rh (plus for two atoms and minus for another two) and $1.0\cdot 10^{-4}$ μ_B for Ge. Thus each atom in RhGe has a complicated magnetic pattern and can be considered as an atomic-size Skyrmion. The calculated toroidal moment for Rh is of about $2.6\cdot 10^{-4}\mu_B$ whereas for Ge it is only $0.2\cdot 10^{-4}\mu_B$. In these calculations vector $\mathbf{r}$ is in dimensionless crystallographic units (and therefore both Q_{jk} and $\mathbf{T}$ have the dimension of μ_B).

Our calculations of possible magnetic ordering in RhGe with the $B20$ structure are mainly illustrative rather that quantitative. However, they allow us to understand the physical picture behind them. Both Rh and Ge atoms possess 'antiferromagnetically' distributed local spin densities with quadrupole and toroidal magnetic moments regularly ordered inside the unit cell. The plus and minus magnetization directions are slightly canted (probably owing to the spin-orbit Dzyaloshinskii-Moriya interactions). Since these cants governed by the crystal symmetry are regular, small ferromagnetic moments emerge both for each atom and for the unit cell as a whole. Different orientations of $\mathbf{M}(\mathbf{r})$ for different atoms can be observed in magnetic neutron or x-ray diffraction via $h00$, $0k0$, $00l$ forbidden reflections with odd h, k or l.

It is possible what both the low-temperature superconducting state and magnetic ordering may be explained by mixing s- and p-wave state. Since the net ferromagnetic moments are weak, they should not be devastating for superconductivity. From the other side, the possible role of toroidal moments in superconductivity is discussed for many years [46, 47] and our findings could bring a new dimension to those discussions.

Of course, the suggested picture of magnetic ordering is oversimplified because it does not include possible helimagnetic spiraling typical of the noncentrosymmetric $B20$ structures. Perhaps more sophisticated pseudopotentials and the Hubbard U interaction should be used for a more quantitative description of magnetism in RhGe.

In conclusion, we have discovered an unusual coexistence of superconductivity and magnetism in the noncentrosymmetric RhGe crystal. An importance of the spin-orbit interactions for non-collinear magnetization distributions characterized by magnetic quadrupole, toroidal, and spin-hedgehog-like patterns is demonstrated with *ab initio* simulations. Our findings provide a basis for the further studies of noncentrosymmetric magnetic superconductors.

The authors are grateful to S. M. Stishov, for support of this work and for helpful discussion. A. V. T. thanks A.V. Nikolaev and D.A. Salamatin for helpful discussion. The work was supported by the Russian Foundation for

Basic Research (grants No. 14-02-00001), the Russian Science Foundation (grant RSF-14-22-00093) and by special programs of the Department of Physical Science, Russian Academy of Sciences.

[1] D. D. Osheroff, R. C. Richardson, and D. M. Lee, Phys.Rev. Lett. **28**, 885 (1972).

[2] D. Vollhardt and P. Wolfle, 1990, *The Superfluid Phases of Helium 3* (Taylor & Francis, London).

[3] J. Bardeen, L. N. Cooper, and J. R. Schrieffer, Phys.Rev. **108**, 1175 (1957).

[4] C. Pfleiderer, Rev. Mod. Phys., **81**, 1551 (2009).

[5] P. W. Anderson Phys. Rev. B **30**, 1549 (1984).

[6] S.S. Saxena, P. Agarwal, K. Ahilan, F.M. Grosche, R.K.W. Hasselwimmer, M.J. Steiner, E. Pugh, I.R. Walker, S.R. Julian, P. Monthoux, G.G. Lonzarich, A. Huxley, I. Sheikin, D. Braithwaite, and J. Flouquet, Nature (London) **604**, 587 (2000).

[7] D. Aoki, A. Huxley, E. Ressouche, D. Braithwaite, J. Flouquet, J-P. Brison, E. Lhotel & C. Paulsen Nature (London) **413**, 613 (2001).

[8] N. T. Huy, A. Gasparini, D. E. de Nijs, Y. Huang, J.C.P. Klaasse, T. Gortenmulder, A. de Visser, A. Hamann, T. Görlach, and H. v. Löhneysen, Phys. Rev. Lett. **99**, 067006 (2007).

[9] V.P. Mineev , Int. J. Modern Physics B, **18**, 1 (2004).

[10] K. V. Samokhin, E. S. Zijlstra, and S. K. Bose, Phys.Rev. B, **69**, 094514 (2004).

[11] V.M. Edel'shtein, Zh. Eksp. Teor. Fiz. **95**, 2151 (1989) [JETP **68**, 1244 (1989)]; V.M. Edelstein, Phys. Rev. Lett. **75**, 2004 (1995).

[12] L.P. Gor'kov and E.I. Rashba, Phys. Rev. Lett.**87**, 037004 (2001).

[13] E. Bauer, G. Hilscher, H. Michor, Ch. Paul, E.W. Scheidt, A.Gribanov, Yu. Seropegin, H. Noe.l, M. Sigrist, and P. Rogl, Phys. Rev. Lett. **92**, 027003 (2004).

[14] P.A. Frigeri, D.F. Agterberg, A. Koga, and M. Sigrist, Phys. Rev. Lett. **92**, 097001 (2004).

[15] Akazawa, T., H. Hidaka, T. Fujiwara, T. C. Kobayashi, E.Yamamoto, Y. Haga, R. Settai, and Y. Onuki, J. Phys.: Condens. Matter **16**, L29 (2004).

[16] C. Pfleiderer, G. J. McMullan, S. R. Julian, and G. G. Lonzarich, Phys. Rev. B **55**, 8330 (1997).

[17] C. Thessieu, C. Pfleiderer, and J. Flouquet, Physica B **239**, 67 (1997).

[18] V.I. Larchev, S.V. Popova, J. Less-Common Metals,**87**, 53 (1982).

[19] Y. Ishikawa and M. Arai, J. Phys. Soc. Jpn. **53**, 2726 (1984).

[20] J. Thompson, Z. Fisk, and G. Lonzarich, Physica B **161**, 317 (1989).

[21] C. Pfleiderer, D. Reznik, L. Pintschovius, H. v. Lohneysen, M. Garst, and A. Rosch, Nature (London) **427**, 227 (2004).

[22] S. Mühlbauer, B. Binz, F. Jonietz, C. Pfleiderer, A. Rosch, A. Neubauer, R. Georgii, and P. B.oni, Science **323**, 915 (2009).

[23] X. Z. Yu, Y. Onose, N. Kanazawa, J. H. Park, J. H. Han, Y. Matsui, N. Nagaosa, and Y. Tokura, Nature (London) **465**, 901 (2010).

[24] A. Neubauer, C. Pfleiderer, B. Binz, A. Rosch, R. Ritz, P. G. Niklowitz, and P. B.oni, Phys. Rev. Lett. **102**, 186602 (2009).

[25] M. Lee, W. Kang, Y. Onose, Y. Tokura, and N. P. Ong, Phys. Rev. Lett.**102**, 186601 (2009).

[26] R. Ritz, M. Halder, C. Franz, A. Bauer, M. Wagner, R. Bamler, A. Rosch, and C. Pfleiderer, Phys. Rev. B **87**, 134424 (2013).

[27] H. Takizawa, T. Sato, T. Endo, and M. Shimada, J. Solid State Chem.**73**, 40 (1988).

[28] N. Kanazawa, Y. Onose, T. Arima, D. Okuyama, K. Ohoyama, S.Wakimoto, K. Kakurai, S. Ishiwata, and Y. Tokura, Phys. Rev. Lett. **106**, 156603 (2011).

[29] O. L. Makarova, A. V. Tsvyashchenko, G. Andre, F. Porcher, L. N. Fomicheva, N. Rey, and I. Mirebeau, Phys. Rev. B **85**, 205205 (2012).

[30] M. Deutsch, O. L. Makarova, T. C. Hansen, M. T. Fernandez-Diaz, V. A. Sidorov, A. V. Tsvyashchenko, L. N. Fomicheva, F. Porcher, S. Petit, K. Koepernik, U. K. Rössler, and I. Mirebeau, Phys. Rev. B **89**, 180407(R) (2014).

[31] S. V. Grigoriev, N. M. Potapova, S.-A. Siegfried, V. A. Dyadkin, E.V. Moskvin, V. Dmitriev, D. Menzel, C. D. Dewhurst, D. Chernyshov, R. A. Sadykov, L. N. Fomicheva, and A.V. Tsvyashchenko, Phys. Rev. Lett. **110**, 207201 (2013).

[32] K. Shibata, Z. X. Yu, T. Hara, D. Morikawa, N. Kanazawa, K. Kimoto, S. Ishiwata, Y. Matsui, and Y. Tokura, Nat. Nanotechnol.**8**, 723 (2013).

[33] L.G. Khvostantsev, V.N. Slesarev and V.V. Brazhkin, High Pressure Research, **24**, 371 (2004).

[34] A.C. Larson, R.B. Von Dreele, (1987) General Structure Analysis System (GSAS), Los Alamos National Laboratory, Report LAUR 86-748 (2000).

[35] B.H. Toby, J. Appl. Crystallogr. **34**, 210 (2001).

[36] See the Supplemental Material at http:// for experimental details and technical procedures.

[37] A. H. Wilson, Proc. R. Soc. London A **167**, 580 (1938).

[38] J. F. DiTusa, S. B. Zhang, K. Yamaura, Y. Xiong, J. C. Prestigiacomo, B. W. Fulfer, P. W. Adams, M. I. Brickson, D. A. Browne, C. Capan, Z. Fisk, and Julia Y. Chan, Phys. Rev. B **90**, 144404 (2014).

[39] B. T. Mathias, T. H. Geballe, and V. B. Compton, Rev. Mod. Phys. **35**, 1 (1963).

[40] N. Tateiwa, T. C. Kobayashi, T. Amaya, Y. Haga, R. Settai, Y. Onuki, Phys. Rev. B **69**, 180513 (2004).

[41] A. E. Petrova, V. A. Sidorov, and S. M. Stishov, Physica B **359-361**, 1463 (2005).

[42] P. Giannozzi, S. Baroni, N. Bonini, M. Calandra, R. Car, C. Cavazzoni, D. Ceresoli, G. L. Chiarotti, M. Cococcioni, I. Dabo, A. Dal Corso, S. Fabris, G. Fratesi, S. de Gironcoli, R. Gebauer, U. Gerstmann, C. Gougoussis, A. Kokalj, M. Lazzeri, L. Martin-Samos, N. Marzari, F. Mauri, R. Mazzarello, S. Paolini, A. Pasquarello, L. Paulatto, C. Sbraccia, S. Scandolo, G. Sclauzero, A. P. Seitsonen, A. Smogunov, P. Umari, R. M. Wentzcovitch, J. Phys. Condens. Matter **21**, 395502 (2009).

[43] The Quantum ESPRESSO pseudopotential data base: `http://www.quantum-espresso.org/pseudopotentials`

[44] I. Dzyaloshinskii, Solid State Comm. **82**, 579 (1992).
[45] I. B. Khriplovich and S. K. Lamoreaux. *CP* Violation Without Strangeness. Electric Dipole Moments of Particles, Atoms, and Molecules. Springer, New York, 1997; p. 157.
[46] V. L. Ginzburg, A.A Gorbatsevich, Yu.V. Kopaev, and B.A. Volkov, Solid State Commun. **50**, 339 (1984).
[47] Yu. V. Kopaev, Physics – Uspekhi, **52**, 1111 (2009).

Supplemental materials to the manuscript

I. EXPERIMENTAL AND SIMULATION DETAILS

The new polymorph of RhGe with FeSi ($B20$) structure was obtained by melting reaction of the constituent materials at 8 GPa and 1700 K. Its powder XRD pattern was collected on HUBER (G670) diffractometer with Cu Kα_1 radiation in the transmission mode, at 2θ step 0.005° in the angular range from 4 to 95 degrees at room temperature and normal pressure. The crystal structure was refined by Rietveld full-profile analysis of XRD pattern, using [S1, S2] programs. It crystallizes in simple cubic, space group $P2_13$ (No. 198) with a=4.85954(2) Å (see Fig. S1). The unit cell volume ($V = 114.758(1)$ Å^3) of B20 cubic phase of RhGe is 4.6% less than the unit cell volume ($V = 120.042$ Å^3) of normal pressure phase with the orthorhombic ($B31$) MnP-type structure [S3].

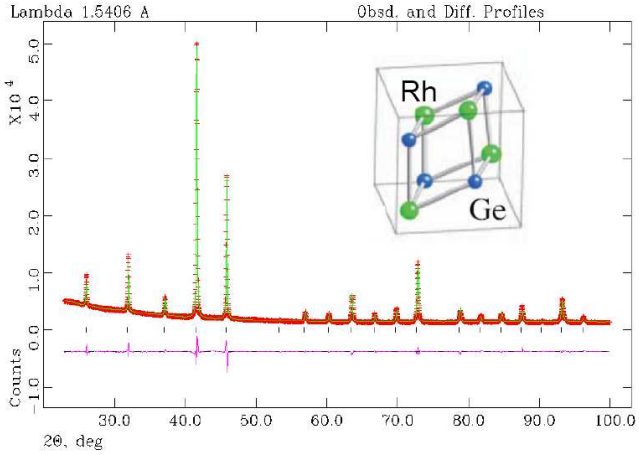

FIG. S1: X-ray Rietveld refinement of $RhGe_{0.986}$ ($R_F = 0.0188$, $R_P = 0.0260$, $R_{WP} = 0.0418$). The observed (+), calculated (solid line) and difference between observed and calculated (bottom curve) powder diffraction profiles. The positions of all allowed Bragg reflections are indicated by the vertical tick marks. Insert: the crystal structure of $B20$-type RhGe.

Structural, electronic and magnetic properties of the RhGe crystals of B20 and MnP types were quantitatively evaluated with the Quantum ESPRESSO package [S4]. The scalar relativistic pseudopotentials `Rh.pbesol-spn-kjpaw_psl.0.2.3.UPF` and `Ge.pbesol-dn-kjpaw_psl.0.2.2.UPF` were used for structure optimization (all the pseupotentials used in this work were taken from the Quantum ESPRESSO data base [S5]). The calculated energy-vs-volume dependence for RhGe is shown in Fig. S2. The $B20$ structure is more dense and it becomes energetically favorable for pressure above circa 8 GPa (at $T = 0$). The atomic parameters u demonstrate rather strong pressure dependence and the Rh sublattice is more changeable than the Ge sublattice (see the insertion in Fig. S2). This may be important for the electron-phonon interaction responsible for superconductivity. For very high pressures, the atomic parameters tend to their ideal values u(Rh) = 1-u(Ge) = $1/(4\tau) \approx 0.1545085$ ($\tau = (1+\sqrt{5})/2$ is the golden mean) which correspond to the perfect structure of a crystalline approximant of icosahedral quasicrystals [S6]. From the physical point of view those values provide the densest packing of equal spheres in the B20 structure [S7]. An additional finding from the DFT simulations is that the $B20$ phase remains stable relative to the transition into the $B2$ primitive cubic phase (the $Pm3m$ space group) even at very high pressure.

Fully relativistic GGA pseudopotentials `Rh.rel-pbesol-spn-kjpaw_psl.0.2.3.UPF` and `Ge.rel-pbesol-dn-kjpaw_psl.0.2.2.UPF` were used for searching possible non-collinear magnetic structures with the spin-orbit interaction. We have also tried the so-called ultra-soft (US) potentials `Rh.rel-pbesol-spn-rrkjus_psl.0.2.3.UPF` and `Ge.rel-pbesol-dn-rrkjus_psl.0.2.2.UPF` which provide more quick convergence of the DFT process. However the magnetic effects have been found to be very subtle in the case of the US potentials and we will not present here the results obtained with them.

It is expected from the cubic symmetry of the $B20$ phase that the preferable orientation of the total magnetization $\langle \mathbf{M}(\mathbf{r}) \rangle$ (averaged over the unit cell) should be either {001} or {111}. Both cases have been calculated using initial magnetizations of Rh and Ge atoms with the corresponding symmetries and the {001} orientation is found to be slightly more preferable. The magnitudes of the initial magnetizations are chosen to be of the order of μ_B or less, and directed along the {001} axis with the same or opposite signs for Rh and Ge atoms; in all cases they converge to similar final values. It should be emphasized that even if the value of initial magnetization is very small the

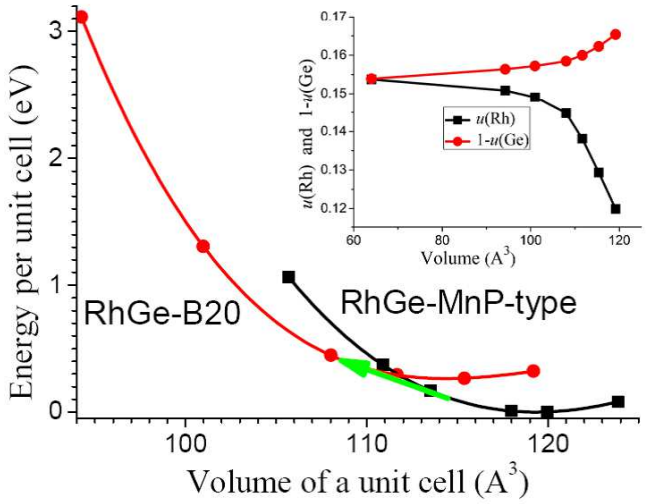

FIG. S2: Calculated energy vs the unit cell volume for metastable ($B20$) and stable (MnP-type) phases of RhGe. The common tangent line (shown as an arrow) determines the transition pressure (about 8 GPa) and the volume change at the transition point (about 6%). Zero energy corresponds to the MnP-type phase at zero pressure. Insert: changes of the Rh and Ge atomic parameters u in the $B20$ phase.

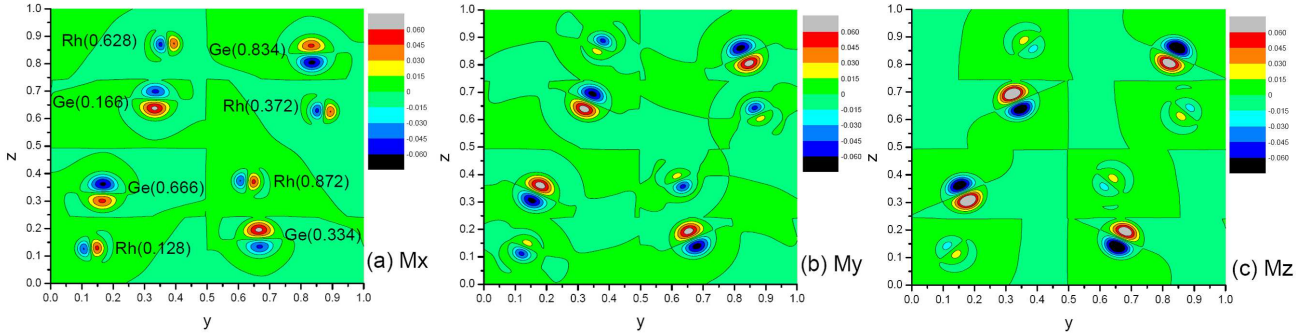

FIG. S3: Magnetic moment distribution inside the RhGe unit cell viewing along the x-axis (Quantum Espresso simulations). Space distributions of (a) M_x-, (b) M_y-, and (c) M_z-components of magnetic moments are shown in the yz-planes passing through the centers of corresponding atoms. Each figure is composed from 8 patches showing the magnetization distributions around the corresponding atoms at 8 different x-levels; the atomic symbols and the x-levels of those patches are indicated only for (a). The boundaries between the patches are the straight lines: $y = 0.5$, $z = 0.25$, $z = 0.5$, and $z = 0.75$. The color scale palette is in arbitrary units.

magnetization $\mathbf{M}(\mathbf{r})$ does not converge to zero. Instead, the average absolute magnetization $\langle|\mathbf{M}(\mathbf{r})|\rangle$ grows during the self-consistent energy minimization process so that the final magnetization distribution has cubic symmetry with zero average magnetization $\langle\mathbf{M}(\mathbf{r})\rangle$. However this cubic distribution has a slightly higher energy than the distribution resulting from the uniaxial initial magnetization and we will not present its structure here. In all cases, the self-consistent process started from a superposition of atomic orbitals plus a superimposed 'randomization' of atomic orbitals suggested by Quantum Espresso.

A typical example of the relaxed magnetization distribution inside a unit cell is shown in Fig. S3. Both Rh and Ge atoms demonstrate quickly alternated patterns of inhomogeneous magnetization so that their average magnetization is rather small. The tensor of magnetization directions $D_{ik} = \langle M_i(\mathbf{r})M_k(\mathbf{r})\rangle_{sph}$ better characterizes distribution of the magnetization near atoms than $\langle|\mathbf{M}(\mathbf{r})|\rangle_{sph}$ because describes also the preferable direction of the magnetization. For Rh atom

$$D(\mathrm{Rh}) = \begin{pmatrix} 1.5 & 0.5 & 0.3 \\ 0.5 & 2.5 & -0.1 \\ 0.3 & -0.1 & 0.2 \end{pmatrix} \cdot 10^{-8}\ \mu_B^2$$

The tensor components of $D_{ik}(\mathrm{Rh})$ show that the Rh moments are preferably oriented in the xy plane because

D_{xx}(Rh) and D_{yy}(Rh) are larger than all other tensor components.

In contrast, for Ge all the tensor components are of the same order of magnitude

$$D(\mathrm{Ge}) = \begin{pmatrix} 7.6 & -5.2 & -3.6 \\ -5.2 & 6.5 & 4.7 \\ -3.6 & 4.7 & 11.5 \end{pmatrix} \cdot 10^{-8}\ \mu_B^2$$

and they are larger than for Rh; this correlates with stronger absolute magnetization of Ge atoms clearly visible in Fig. S3.

[S1] A.C. Larson, R.B. Von Dreele, (1987) General Structure Analysis System (GSAS), Los Alamos National Laboratory, Report LAUR 86-748 (2000).

[S2] B.H. Toby, J. Appl. Crystallogr. **34**, 210 (2001).

[S3] B. T. Mathias, T. H. Geballe, and V. B. Compton, Rev. Mod. Phys. **35**, 1 (1963).

[S4] P. Giannozzi, S. Baroni, N. Bonini, M. Calandra, R. Car, C. Cavazzoni, D. Ceresoli, G. L. Chiarotti, M. Cococcioni, I. Dabo, A. Dal Corso, S. Fabris, G. Fratesi, S. de Gironcoli, R. Gebauer, U. Gerstmann, C. Gougoussis, A. Kokalj, M. Lazzeri, L. Martin-Samos, N. Marzari, F. Mauri, R. Mazzarello, S. Paolini, A. Pasquarello, L. Paulatto, C. Sbraccia, S. Scandolo, G. Sclauzero, A. P. Seitsonen, A. Smogunov, P. Umari, R. M. Wentzcovitch, J. Phys. Condens. Matter **21**, 395502 (2009).

[S5] The Quantum ESPRESSO pseudopotential data base: `http://www.quantum-espresso.org/pseudopotentials`

[S6] V.E. Dmitrienko. J. Phys. France. **51**, 2717 (1990).

[S7] V.E. Dmitrienko. Acta Cryst. A **50**, 515 (1994).